Effects of phase lag on the hovering flight of damselfly and dragonfly

Pei-Yi Zou,[1] Yu-Hsiang Lai,[2] and Jing-Tang Yang[1,2,*]

[1]*Department of Engineering Science and Ocean Engineering, National Taiwan University, 10617 Taipei, Taiwan*

[2]*Department of Mechanical Engineering, National Taiwan University, 10617 Taipei, Taiwan*

(Received 30 April 2019; revised manuscript received 16 August 2019; published 4 December 2019)

In this work we studied the differences in flight kinematics and aerodynamics that could relate to differences in wing morphologies of a dragonfly and a damselfly. The damselflies and dragonflies normally fly with the fore wing or hind wing in the lead, respectively. The wing of the damselfly is petiolate, which means that the wing root is narrower than that of the dragonfly. The influence of the biological morphology between the damselfly and the dragonfly on their hovering strategies is worthy of clarification. The flight motions of damselflies and dragonflies in hovering were recorded with two high-speed cameras; we analyzed the differences between their hovering motions using computational fluid dynamics. The distinct mechanisms of the hovering flight of damselflies (*Matrona cyanoptera*) and dragonflies (*Neurothemis ramburii*) with different phase lags between fore and hind wings were deduced. The results of a comparison of the differences of wing phases in hovering showed that the rotational effect has an important role in the aerodynamics; the interactions between fore and hind wings greatly affect their vortex structure and flight performance. The wake of a damselfly sheds smoothly because of slender petiolation; a vertical force is generated steadily during the stage of wing translation. Damselflies hover with a longer translational phase and a larger flapping amplitude. In contrast, the root vortex of a dragonfly impedes the shedding of wake vortices in the upstroke, which results in the loss of a vertical force; the dragonfly hence hovers with a large amplitude of wing rotation. These species of Odonata insects developed varied hovering strategies to fit their distinct biological morphologies.

DOI: 10.1103/PhysRevE.100.063102

I. INTRODUCTION

The flight abilities of birds and insects have generated a deep concern in observers. Because of physical limitations, only a few birds have adopted special mechanisms to hover [1–4], whereas a damselfly and a dragonfly can hover well. The agile and enduring flight abilities of damselflies and dragonflies have made them successful predators in nature. Their four-winged feature enables control and maneuverability better than for other flyers with two wings. With an increasing interest in the aerobiomechanics of insects, dragonflies have become ideal research subjects because of their striking flight performances.

Norberg [5] filmed dragonflies hovering in the field; he carefully recorded and analyzed their wing motion, which laid the foundations for subsequent mechanical and numerical studies. Dragonflies have been generally reported to vary their flight speed by adjusting the phase between fore and hind wings [6]. Phase lags of three types are generally used. In takeoff or acceleration, dragonflies fly with an in-phase stroke to enhance the production of force [6]; in hovering flight, an out-of-phase stroke is employed [7,8]. In straightforward flight, the hind wing of a dragonfly leads the fore wing with a phase shift [9,10]. The interaction between the fore and hind wings with varied phase lags has been widely investigated [11–14], which showed that a phase lag in a tandem configuration might be an outstanding method to control flight. Conversely, these findings indicate that, although a phase lag of 180° is widely used in the study of a hovering dragonfly, a different phase lag can still be employed in hovering flight. Further investigation of the flow structure with a specific phase lag in hovering flight is warranted.

Wang and Russell [15] used experimental measurements to derive the two-dimensional (2D) wing motion of a hovering dragonfly and applied a numerical method for analysis; they found that being out of phase by 100°−220° can minimize the power consumption and provide a stable body oscillation. Sun and Huang [12] investigated the effects of interaction between fore and hind wings with a phase lag varying in a range −180°−180° at varied flight speeds; they indicated that this interaction with the hind wing in the lead phase had less effect on the performance of the mean total vertical force and the mean total thrust. In contrast, the mean total vertical force apparently declined with the fore wing in the lead phase because of a downward jet produced during the downstroke of the fore wing. Usherwood and Lehmann [16] designed a mechanical model of a "hovering dragonfly" to investigate the aerodynamic efficiency with varied phase lag using digital particle-image velocimetry (2D-DPIV); their results showed that hovering with phase shift 90° (hind wing in the lead) can decrease the power consumption 16% relative to a phase shift −90° (fore wing in the lead) through a swirl removal effect. Those studies might provide an effective explanation why dragonflies use the hind wing in the lead phase in their flight. Lua *et al.* [17] calculated the aerodynamics of 2D flapping wings in a tandem configuration in forward flight; they pointed out that the total thrust generated with a tandem

*Corresponding author: jtyang@ntu.edu.tw

TABLE I. Biological information of a dragonfly (*Neurothemis ramburii*) and a damselfly (*Matrona cyanoptera*) in hovering.

	Damselfly (mean ± SEM)	Dragonfly (mean ± SEM)
Mass (g)	0.139 ± 0.013	0.142 ± 0.012
Length (cm)	6.500 ± 0.183	4.100 ± 0.087
Span of fore wing (cm)	4.400 ± 0.054	3.300 ± 0.033
Span of hind wing (cm)	4.400 ± 0.054	3.300 ± 0.033
Chord of fore wing at midwing (cm)	1.200 ± 0.030	0.800 ± 0.017
Chord of hind wing at midwing (cm)	1.300 ± 0.030	1.100 ± 0.060

configuration can be either detrimental or beneficial relative to two isolated single wings. This effect relies on how and when the hind wing interacts with the wake of the fore wing. Hefler *et al.* [18] investigated the interwing interaction along the wingspan under tethered and free-flying conditions; they indicated that the effects of the interactions varied along the four spanwise regions of the hind wing. In the region near the wing root, the leading-edge vortex (LEV) of the hind wing cannot develop well because of a small translational distance; in the inner region of the wing, a distinct LEV-LEV synergy can enhance the circulation of the hind wing. In the transition region, the downwash induced from the fore wing might dominate the LEV interactions. In the outer region, the hind wing can capture the shed vortex of the fore wing, which can assist to form a LEV in the last quarter of the stroke. These results revealed that the varied aerodynamic interactions in spanwise regions of a wing have an apparent variation with a particular phase.

The flight of a damselfly is much less discussed than that of a dragonfly. Wakeling and Ellington [19] reported studies to reveal the differences in the free flight of dragonflies and damselflies; they explored the fact that a dragonfly, which flew with the hind wing in the lead, had greater wing-beat frequencies and greater velocities and accelerations than a damselfly. The dragonfly flapped with a fixed inclination of the stroke plane, which was subject to the body axis. In contrast, the damselfly, which flew with the fore wing in the lead, had larger variations in the angle of the stroke plane and performed superior nondimensional velocities and accelerations. Bode-Oke *et al.* [20] used numerical simulation to explain the flight mechanism of a damselfly during a nonjumping takeoff; they found that the interaction between the fore and hind wings could assist the damselflies to increase lift and thrust during takeoff. In addition, most authors have focused on the effect of an aerodynamic force and discuss separately the effects of the morphology [21,22] and the kinematics [7–9,11–15,17,20]. The correlation between the wing morphology and wing kinematics is also less discussed.

Although a dragonfly and a damselfly have strongly similar geometries, they have significant differences. Apart from their flight motions, the wing morphologies also differ. The wing of a damselfly has a petiolation greater than that of a dragonfly. It is of interest to understand how the differences in flight kinematics and aerodynamics could correspond to differences in wing morphologies of a dragonfly and damselfly. The reasons that these two species adopt different hovering motions have not been thoroughly interpreted. Moreover, in many preceding studies the flapping of fore and hind wings of a dragonfly has been mimicked through simplified mechanisms; the lift and drag were measured to compare with a single-wing situation [13,23–25] or simplified models were used to simulate the wing motion. The discussion of the effect of phase lag based upon the real biological perception is, however, insufficient. In this work, our purpose was to compare the differences in hovering kinematics and aerodynamics between the dragonfly and damselfly. We analyzed the effect of phase lag considering the flight motion of the damselfly and the dragonfly, using numerical simulation to provide the three-dimenisonal (3D) flow features and the difference in force generation. We consequently explain how the different hovering kinematics effectively provide lift with distinct wing morphology between the damselfly and the dragonfly.

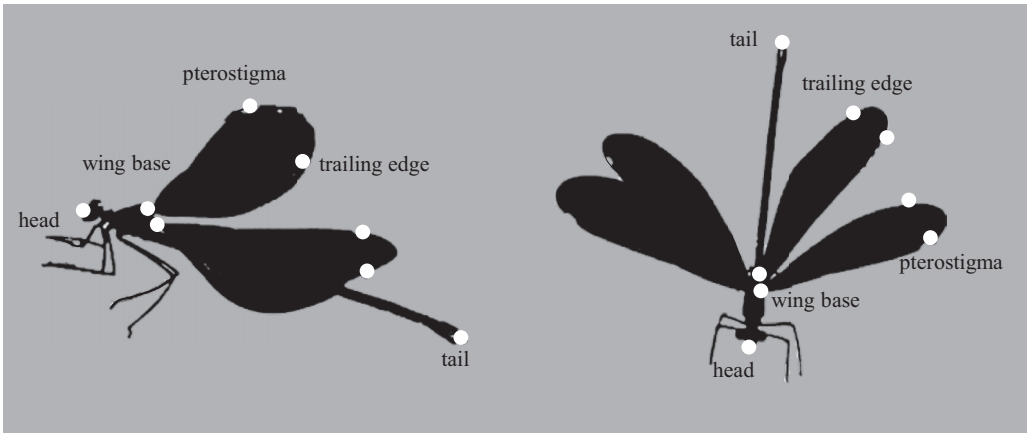

FIG. 1. Feature points marked on the wing surface of a damselfly (*Neurothemis ramburii*).

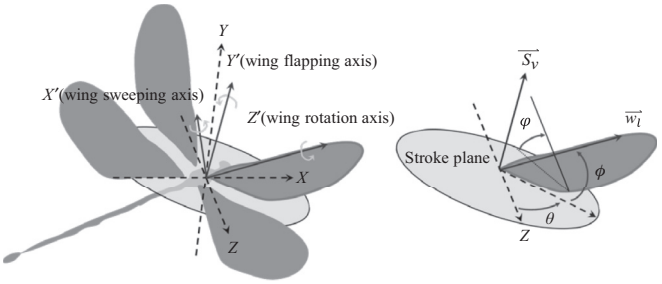

FIG. 2. Definitions of wing kinematics described with three Euler angles with respect to the mean stroke plane: flapping angle θ, rotation angle φ, and sweeping angle ϕ.

II. METHOD

A. Experimental setup

Nineteen damselflies (*Matrona cyanoptera*) and ten dragonflies (*Neurothemis ramburii*) were captured. We carefully made more than 30 experimental films and chose the hovering motions of five damselflies and three dragonflies. The biological information was measured and is shown in Table I. The flight motions of damselflies and dragonflies in hovering were recorded in a transparent experimental chamber ($80 \times 35 \times 60\,\mathrm{cm}^3$) with two synchronized high-speed cameras (Phantom v7.3 and Phantom v310), aligned orthogonally. The resolutions of the cameras were 1024×1024 pixels; 1000 and 2000 fps were used to capture the flight motion of damselflies and dragonflies, respectively. To capture accurately the hovering motion, we hung several small toys, bugs, and a few branches in the chamber to attract the damselflies and dragonflies to hover around the hanging objects. The shooting ranges were about 22 cm × 25 cm in side view and 20 cm × 23 cm in top view. In general, —three to five wingbeat cycles could be recorded because of the hovering attitude; a complete and clear wing beat was adopted for analysis. The wing kinematics were measured based on the feature points marked on a wing surface. The three feature points of the wing were marked, respectively, at the pterostigma, that is, the position of the leading edge of the wing; the trailing edge of the wing corresponding to the pterostigma; and the wing root. The two feature points of the body parts were located at the head and the tail (Fig. 1). We first specified manually these points lying on the wings with image-processing software (IMAGEJ), which implemented the kinematic analysis for the sequences of captured images. After deriving the coordinates of the feature points, a program (written in MATLAB) was used to calculate the angles and a fitting function. The same code has been validated and applied to calculate the kinematics of various animals or insects [1,2].

To describe wing kinematics, we considered two Cartesian coordinate systems: a global coordinate system (XYZ) and a wing coordinate system ($X'Y'Z'$). The origin of the global coordinate system was fixed at the wing base, constant with time. Axis X is the direction in which the damselfly flies forward; axis Y is the upward direction vertically and parallel to that of gravity. Axis Z is toward the side of the body, which can serve to define the zero flapping angle. The wing coordinate system is used to describe the wing motion and rotates with wing motion; its origin is also set at the wing base. The sweeping motion is the rotation about axis X'; axis Y' is the rotation axis of the flapping motion. Axis Z' is the wing rotation axis (Fig. 2). Notably, in our work, we assumed that the body posture is fixed and maintains a fixed body angle. The definitions of kinematic variables follow. A mean stroke plane is determined by the average wing-tip trajectories projected to plane XY and calculated with linear regression; the stroke plane must be parallel to the regression line and passes the origin. $\overrightarrow{S_v}$ represents the vector normal to the stroke plane. Flapping angle θ is the angle between the projection of leading-edge vector $\overrightarrow{W_l}$ onto the stroke plane and axis Z. Sweeping angle ϕ is the complementary angle of the angle between $\overrightarrow{W_l}$ and $\overrightarrow{S_v}$. Rotation angle φ is calculated with the rotation of the wing along leading-edge vector $\overrightarrow{W_l}$. The wing kinematic parameters of a dragonfly (*Neurothemis ramburii*) and a damselfly (*Matrona cyanoptera*) in hovering are shown in Table II.

Most previous authors assumed the sweeping angle to be zero and the wings to move only along a stroke plane [7–9,11–17,19,21,23–25,26–32]. The sweeping angle in our work can also be regarded as the deviation angle; these angles have the same definition. Based on several remarks about hovering insects, the mean amplitude of the sweeping angle is within 5° [33,34], which is similar to our observations. Luo *et al.* [35] pointed out that the stroke deviation has an important impact on the cycle-mean aerodynamic force. To ensure the recognition of the effects of the stroke deviation, we took the sweeping angle (deviation angle) of the damselfly and the dragonfly into account in our work.

We used the motion of real damselflies and dragonflies to quantify the flapping and sweeping motions as sinusoidal

TABLE II. Wing kinematic parameters of a dragonfly (*Neurothemis ramburii*) and a damselfly (*Matrona cyanoptera*) in hovering.

	Damselfly (mean)		Dragonfly (mean)	
Frequency (Hz)	14.3		33.1	
Phase lag (deg)	39.6 (fw lead)		68.4 (hw lead)	
Body angle (deg)	18.0		33.8	
	FW	HW	FW	HW
Stroke plane angle (deg)	8.8	14.5	7.1	7.5
Flapping amplitude (deg)	34.2	42.7	28.4	35.5
Sweeping amplitude (deg)	2.6	6.8	4.1	4.2
Rotation amplitude (deg)	57.1	39.2	57.7	54.4

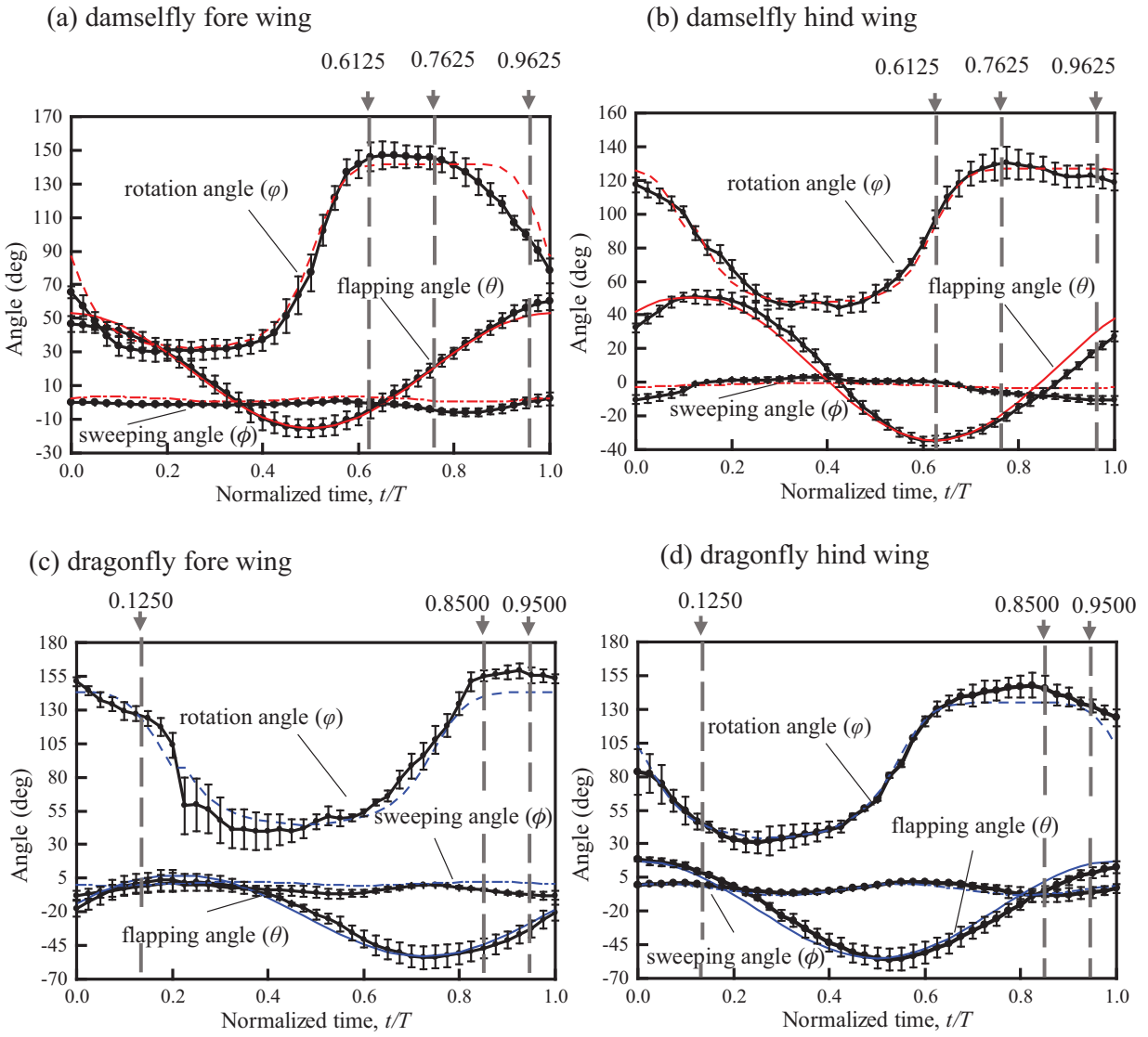

FIG. 3. Wing kinematics and approximate functions of the damselfly and the dragonfly. The normalized time of the damselfly begins at the initiation of the downstroke of the fore wing; the normalized time of the dragonfly begins at the initiation of the downstroke of the hind wing. The dashed line represents the approximate rotation angle; the dotted dashed line represents the approximate sweeping angle; the thin solid line represents the approximate flapping angle.

functions and the rotation motion as a Gaussian distribution. We observed that the rotation motion could be composed of two motions—the translational stage during the midstroke and an abrupt change of rotation angle during the reversal. The shape of a Gaussian function approximates the bell-shaped curve; the top and bottom of the curve can serve to describe the translational stage on adjusting the parameters, and the sides of the curve can describe the rotational stage. In addition, according to our observations, the wing-tip trajectories of the fore and hind wings of the dragonfly have approximately a figure-eight shape; the frequency of the sweeping angle is hence twice that of the flapping angle. For the damselfly, the wing-tip trajectories of the fore wing have approximately a figure-eight shape; the shape of the hind wing is approximately elliptical. The frequency of the fore wing is double that of the hind wing [35]. Because the fore and hind wings of the two species have similar actions, we used the same functions to fit the curves. The wing kinematics and approximate functions of the damselfly and the dragonfly are shown, respectively, in Fig. 3. The motions were described with these equations. The sweeping motion of the hind wing of the damselfly is expressed in Eq. (3),

$$\text{flapping motion}: \theta(t) = A_{f0} - A_f \sin(2\pi f t), \tag{1}$$

$$\text{sweeping motion}: \phi(t) = A_{s0} - A_s \sin(4\pi f t + \text{shift}), \tag{2}$$

$$\text{sweeping motion}: \phi(t) = A_{s0} - A_s \sin(2\pi f t + \text{shift}), \tag{3}$$

$$\text{rotation motion}: \varphi(t) = A_{p0} + \frac{A_p}{1 + \left|\frac{f_{\text{cycle}} - c}{a}\right|^{2b}},$$
$$f_{\text{cycle}} = (ft - \lfloor ft \rfloor) \times 10, \tag{4}$$

TABLE III. Relevant parameters of approximate functions with flapping, sweeping, rotation motion.

	Damselfly		Dragonfly	
	Fore wing	Hind wing	Fore wing	Hind wing
A_{f0} (deg)	19.0	7.9	−23.0	−19.0
A_f (deg)	34.0	42.5	30.0	36.0
A_{s0} (deg)	2.0	−2.0	1.0	−4.0
A_s (deg)	1.5	1.5	1.5	4.0
Shift	0.29	0.26	0.25	0.32
A_{p0} (deg)	31.9	46.9	43.0	33.0
A_p (deg)	110	80	100	102
a	2.5	2.6	2.4	2.5
b	3.6	3.8	2.8	3.0
c	5.0	5.0	5.0	5.0

in which appear time t, flapping frequency f, and motion amplitude and midpoint A, A_0; subscripts p, s, and f denote the rotation, sweeping, and flapping motions, respectively. Parameters a, b, c, and *shift* were used to adjust the rotation and sweeping motion. Floor function ft is a function that takes as input a real number t and gives as output the greatest integer less than or equal to t, denoted floor $(ft) = \lfloor ft \rfloor$. Parameter f_{cycle} was set to split the dimensionless time so that we can use a different Gaussian function to represent the rotation motion, which makes the rotation motion nearer that of the real insects. The relevant parameters of approximate functions, slightly different from that of the real motion, are shown in Table III. To validate the tracking algorithm, we analyzed the real and prescribed motions at varied normalized time in one wingbeat cycle (shown in Figs. 4 and 5). Notably, the prescribed motion is given based on an approximate function of average real motions, with the real motion based on one set of measurement data. There might therefore occur slight differences in the flight motion, but in general, a consistency is maintained that shows the credibility of the tracking algorithm.

B. Numerical method

In our work, two workstations were used to perform the numerical calculations. The specifications follow: processor–Intel Xeon CPU E5-2650 2.20 GHz, RAM–128 GB, HDD–4 TB; processor–Intel Core i9-9980XE CPU 3.00 GHz, RAM–128 GB, HDD–4 TB. The motion of a damselfly and a dragonfly in hovering flight was simulated with commercial software (ANSYS WORKBENCH 14.0); much research on the flapping wing has confirmed the reliability of this software [26–28]. The computational fluid-dynamic (CFD) models of a damselfly and a dragonfly were then created to study their transient flow field. The computational domains comprise three parts, shown in Fig. 6. The outer domain is a cylinder of diameter 56 cm and height 60 cm. The inner domains include two spheres of diameters 20 and 40 cm. The high-resolution mesh in the innermost domain is about 0.06 $\bar{c}$ (mean chord length, $\bar{c} = 0.94$ mm), which ensures the accuracy of the detailed 3D flow structure. The setting has been proved to be sufficiently large [20,36] and was examined with a grid test. Figure 7 shows the difference between three grid points for the vertical force. When the number of grids increases, the vertical force is similar; the setting of 1.46×10^7 grid points was hence employed in our simulation. The body of a model was fixed in the field and only the wings moved with a prescribed average wing motion in hovering. The wing model of the damselfly had fore wing area 0.000 409 m^2 and hind wing area 0.000 412 m^2; the wing model of the dragonfly had fore wing area 0.000 220 m^2 and hind wing area 0.000 289 m^2, shown in Fig. 8. The models of a damselfly and a dragonfly were also simplified here as rigid bodies. The equations governing the flow in the numerical solver were the transient and incompressible continuity equation and the Navier-Stokes equation,

$$\nabla \cdot \boldsymbol{u} = 0, \tag{5}$$

$$\rho \left(\frac{D\boldsymbol{u}}{Dt} \right) = -\nabla P + \mu \nabla^2 \boldsymbol{u} + \boldsymbol{F}, \tag{6}$$

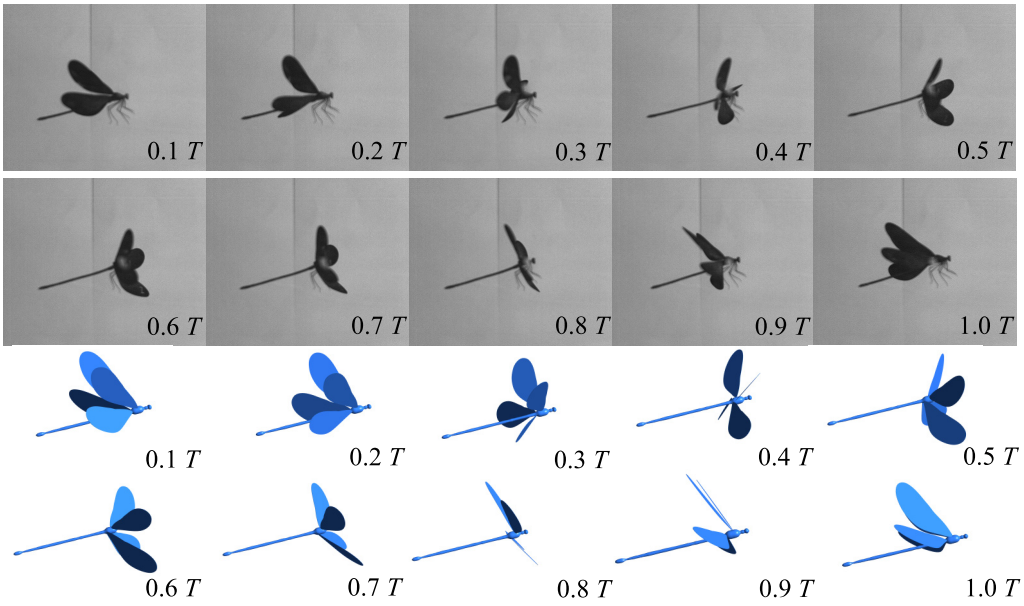

FIG. 4. The real motion (top) and prescribed motion (bottom) of the damselfly at varied normalized time.

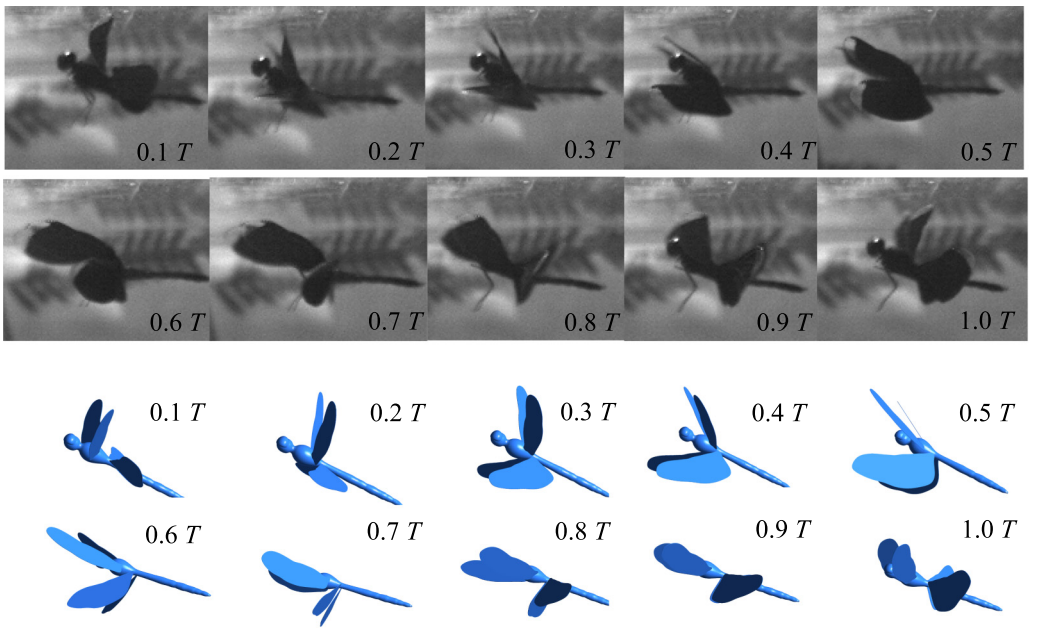

FIG. 5. The real motion (top) and prescribed motion (bottom) of the dragonfly at varied normalized time.

in which appear velocity vector $\boldsymbol{u}$, air density ρ, pressure P, body force vector $\boldsymbol{F}$, and air viscosity μ. For the setting of the boundary conditions, the models of the insects were set as a no-slip wall; the entrance condition was a velocity inlet with zero velocity; the exit condition was regarded as a pressure outlet with zero gauge pressure; the surface of a cylinder was applied as a free-slip wall with zero shear stress. For the solver settings, we applied the SIMPLE scheme for pressure-velocity coupling; the standard scheme was chosen for pressure discretization; the momentum equation was operated with a second-order upwind scheme; the transient formulation was adopted with a first-order implicit scheme. Six wing beats were simulated to allow the flow to stabilize for analysis.

To prescribe the wing motions and to handle complicated grid conditions, we applied a user-defined function (UDF) to compile the program. The three angle motions in hovering were prescribed in macro function DEFINE_CG_MOTION. The velocity and acceleration of a wing were then calculated at every time step. We set up a dynamic mesh to use spring-based smoothing and a remeshing method, which were used together to handle large deformations or large displacements of grid changes.

The Reynolds number ($\mathrm{Re} = U_{\mathrm{tip}}\bar{c}/v$) of the damselfly used in this work was based on a wing-tip velocity ($U_{\mathrm{tip}} = 1.49\,\mathrm{m\,s^{-1}}$) and a mean chord length of the fore wing ($\bar{c} = 0.94\,\mathrm{mm}$) as 900 approximately. The Reynolds number of the dragonfly was about 1600, for which a wing-tip velocity ($U_{\mathrm{tip}} = 2.74\,\mathrm{m\,s^{-1}}$) and a mean chord length of hind wing ($\bar{c} = 0.94\,\mathrm{mm}$) were adopted. Mean vertical force coefficient $\bar{C}_v$, aerodynamic power P_{a}, mean aerodynamic power coefficient $\overline{C_{P_a}}$, and PE (ratio of mean vertical force coefficient

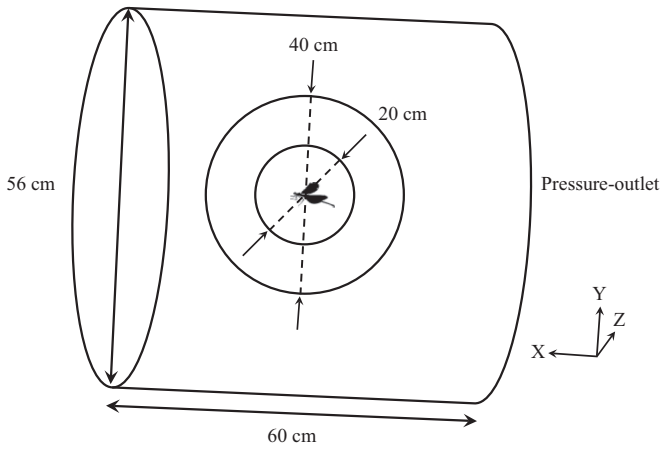

FIG. 6. Physical model of a damselfly in hovering flight.

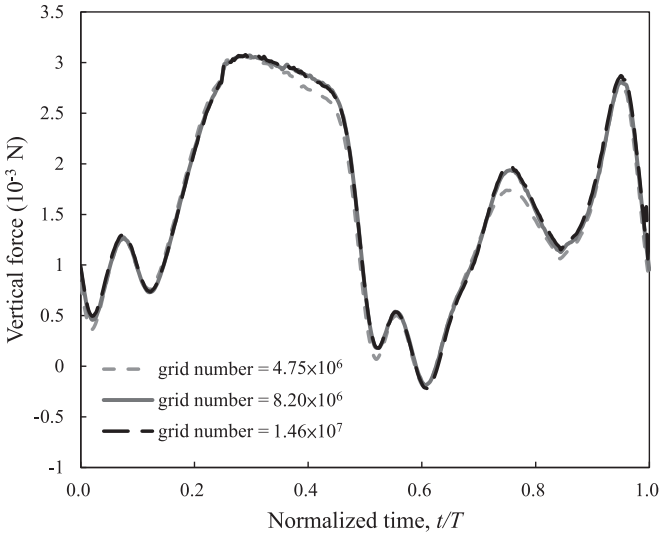

FIG. 7. Grid convergence test with three numbers of grid points.

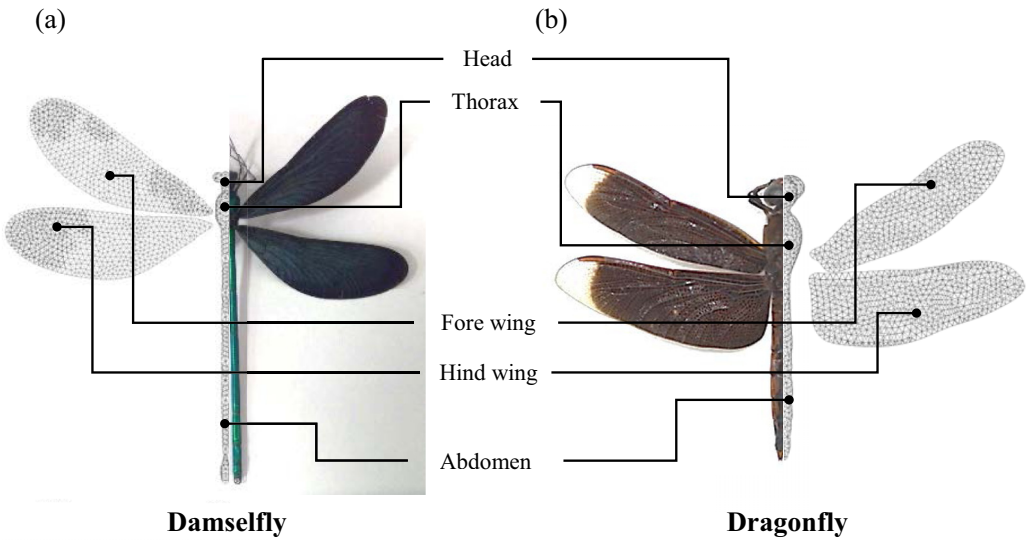

FIG. 8. (a) Figure of damselfly (left) and simulation model with face sizing (right). (b) Figure of dragonfly (left) and simulation model with face sizing (right).

to mean aerodynamic power coefficient), were calculated and defined as follows.

$$\overline{C_v} = \frac{F_v}{0.5\rho U_{\text{tip}}^2 S_w}, \tag{7}$$

$$P_a = -\int \boldsymbol{F} \cdot \boldsymbol{V} dS_w, \tag{8}$$

$$\overline{C_{P_a}} = \frac{P_a}{0.5\rho U_{\text{tip}}^3 S_w}, \tag{9}$$

$$\text{PE} = \frac{\overline{C_v}}{\overline{C_{P_a}}}, \tag{10}$$

in which appear vertical force F_v, wing area of fore wing and hind wing in pairs S_w, and local velocity over the wing surface $\boldsymbol{V}$.

III. RESULTS AND DISCUSSION

A. Flight strategies

Figures 9 and 10 show the wing kinematics of a damselfly and a dragonfly in a cycle recorded from experiment. The wing motion of a hovering insect is divided into four stages: pronation, translational stage during downstroke, supination, and translational stage during upstroke. In the translational stages of the downstroke and upstroke, the wings translate rapidly and with an approximately constant angle of attack; in the pronation and supination stages, the wings rotate sharply along the spanwise axis (leading-edge vector, $\vec{W}_l$). As the wing-wing interaction affects mainly the hind wing, we analyzed the hind wing motion. In a normalized beat cycle of the hind wing of a damselfly (Fig. 9), the four stages were taken to be about 25%, 25%, 22%, and 28%, respectively; in a normalized beat cycle of the hind wing of a dragonfly (Fig. 10), the four stages were taken to be about 31%, 20%, 31%, and 18% of an entire cycle, respectively. These results indicate that the translational stage of a damselfly is longer, about 53% of the entire cycle, whereas a dragonfly has longer pronation and supination stages, which take about 62% of the entire beat cycle.

In Table II, our experimental results show that, during hovering, the fore wing of a damselfly leads by phase shift of 39.6°; the hind wing of dragonfly leads by phase shift of 68.4°. Although these values differ from the generally accepted phase angle, 180°, they are still credible. Sun *et al.* [14] indicated that most current research could show only that the phase lag selected in their work is suitable for the flight mode of the dragonfly studied. For the hovering motion, a damselfly hovers with a smaller wing-beat frequency and larger flapping amplitude. Moreover, the fore and hind wings flap in different inclinations of the stroke plane; this angle is about 8.8° for the fore wing and 14.5° for the hind wing. The fore and hind wing beats of a dragonfly are nearly parallel, as their stroke plane angles are both about 7°. This result that a damselfly has a more variable wing motion than a dragonfly agrees with previous work [19]. Overall, a damselfly flies with a longer translational phase, smaller wing-beat frequency, and larger flapping amplitude, whereas a dragonfly flies with a significant wing rotation, larger wing-beat frequency and a smaller flapping amplitude.

As to wing morphologies, the wing of the damselfly is petiolate; that is, the wing root of the damselfly is narrow and slender, whereas the wing root of the dragonfly is wider than that of the damselfly. The aspect ratios (ARs) of the damselfly and the dragonfly are 4.7, 5.2 in the fore wing, and 4.7, 3.5 in the hind wing. The effects of the wing motion and wing morphologies on the aerodynamic force and the flow structure are discussed further with the simulation results.

B. Aerodynamic performance

A different force generation might result from a different flight strategy, that is, a damselfly flying with the fore wing in the lead but a dragonfly with the hind wing in the lead. Regarding the difference in the wing area and the wing-beat frequency, the vertical force here is dimensionless according

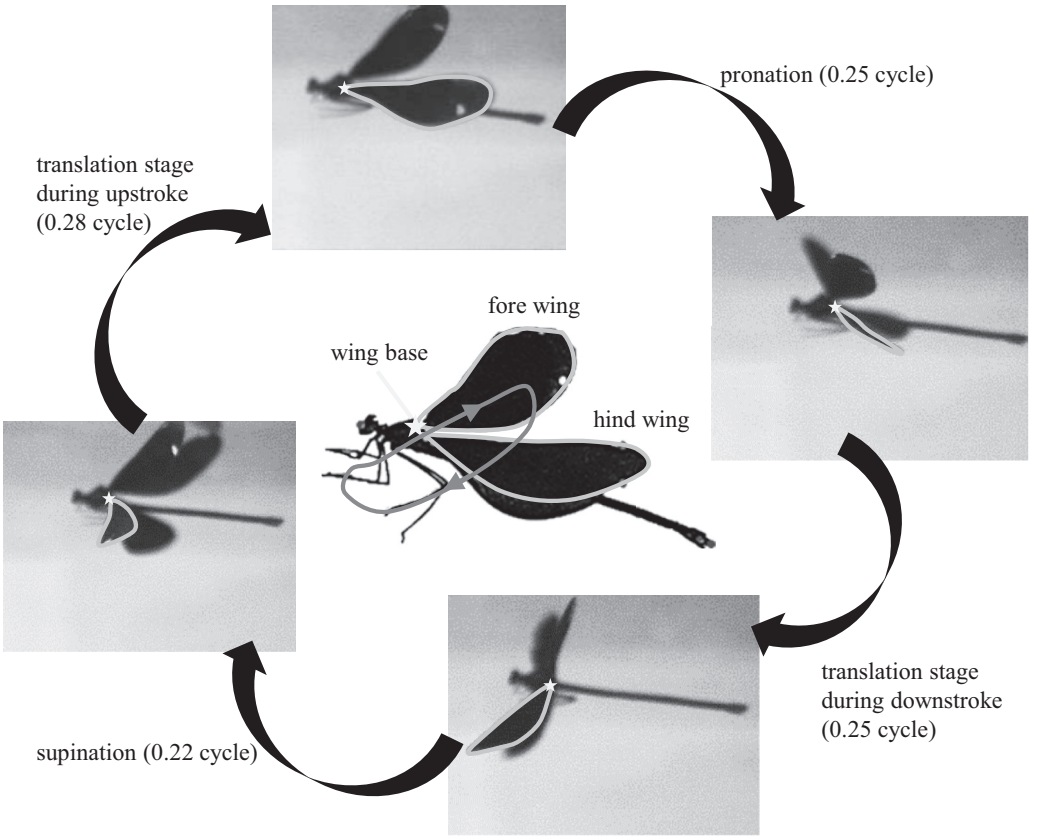

FIG. 9. Analysis of hovering motion in a normalized cycle; the four stages of the hind wing of a damselfly (*Matrona cyanoptera*); an asterisk is used to represent the wing root.

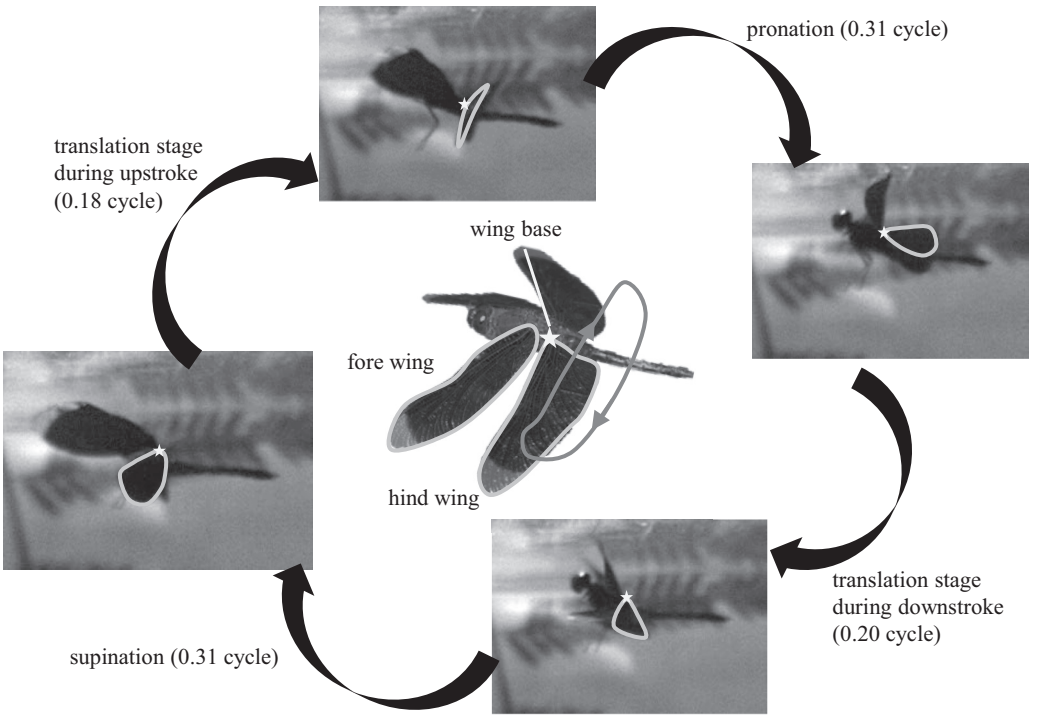

FIG. 10. Analysis of hovering motion in a normalized cycle; the four stages of the hind wing of a dragonfly (*Neurothemis ramburii*); an asterisk is used to represent the wing root.

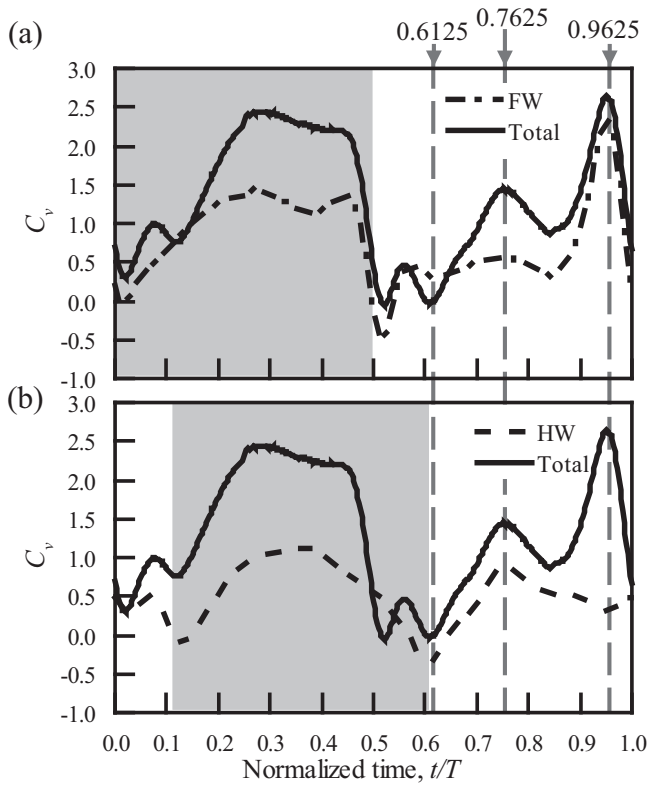

FIG. 11. (a,b) show C_v of the fore and hind wings of a damselfly with dashed lines, respectively; the gray shadings indicate the downstroke.

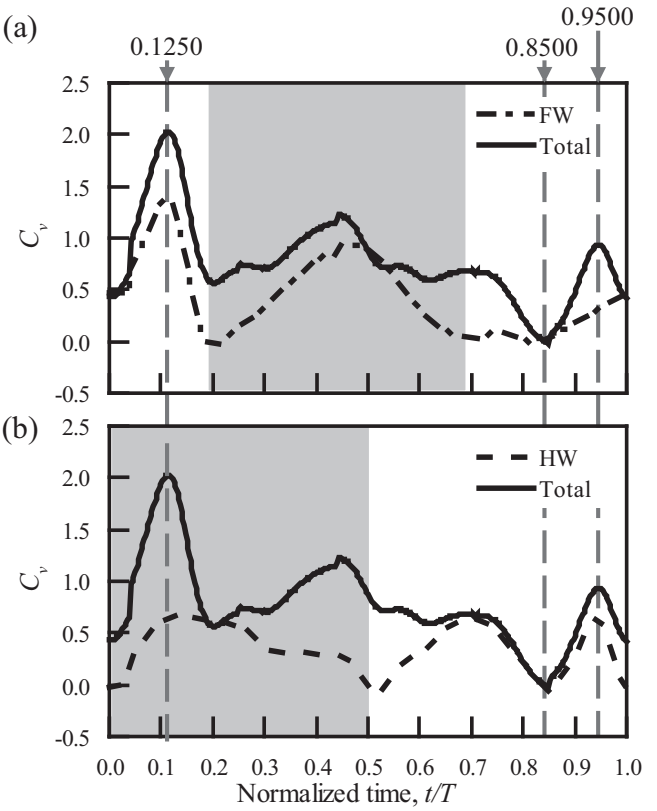

FIG. 12. (a,b) show C_v of the fore and hind wings of a dragonfly with dashed lines, respectively; the gray shadings indicate the downstroke.

to the maximum wing-tip speed and wing area. The vertical force coefficient in one flapping cycle, C_v, is shown in Figs. 11 and 12. The mean vertical force coefficients $\overline{C_v}$ are 1.14 and 1.04 times the weights of the damselfly and dragonfly, respectively; the requirement of the force balance is hence approximately met. The horizontal force is approximately zero. The damselfly has $\overline{C_v}$ larger than that of the dragonfly. The mean aerodynamic power coefficient of the damselfly is 1.14, and for the dragonfly 0.33; the damselfly has PE 0.60 and the dragonfly 0.93. Such results could be discussed in two directions; one is the wing motion and the other is the wing morphology.

Figure 11(a) shows that the rotational effect of the fore wing of a damselfly fluctuates; there is a maximum vertical force at the end of each half stroke. In particular, the maximum C_v appears when the fore wing pronates, but no maximum vertical force appears on the hind wing of a damselfly [Fig. 11(b)]. There is a slight loss of vertical force of both wings at the beginning of each half stroke. In Fig. 12(a), the fore wing of a dragonfly produces no vertical force in the first half of the upstroke, but a maximum vertical force is produced by wing pronation at the end of the upstroke. The hind wing has also a loss of vertical force in the middle of the upstroke; a force is then generated again because of the wing rotation [Fig. 12(b)]. Dickinson and co-workers [29,30] found that the two force maxima occurred at the beginning and end of each half stroke. A rotational circulation was used to explain the force maximum at the end of the half stroke, also named a rotational effect. According to this aerodynamic analysis, the force maxima occur at almost the end of each half stroke in our work. That is, the rotational effect contributes much lift.

According to Phillips *et al.* [21], a greater wing petiolation might produce larger leading-edge vortex (LEV) during the downstroke, which can cause a greater vertical force coefficient. In contrast, the LEV might detach readily on more petiolation during the upstroke. In general, a more petiolate wing could provide greater lift, but would be accompanied with poor aerodynamic efficiency and greater power consumption. Shahzad *et al.* [22] found that a wing with greater aspect ratio and more petiolation could have improved lift performance, but a wing with greater aspect ratio and less petiolation might have a better PE. These studies attained the same conclusion on a petiolate wing. In our work, the damselfly with a petiolate wing has indeed a greater vertical force coefficient but smaller PE. As the motions and the frequency of a damselfly and dragonfly in hovering differ, this result can serve only as a reference. The purpose of our work is to discuss the difference in hovering strategies between the two species. It is difficult to compare the aerodynamic characteristics affected by the wing shape in distinct hovering motions. The influence of the wing shape might be discussed separately from the respective flow structure. The difference of the flow structure between these two insects is discussed as follows.

C. 3D flow structures

To identify how the motion of the fore and hind wings influences the generation of force, we used a CFD simulation

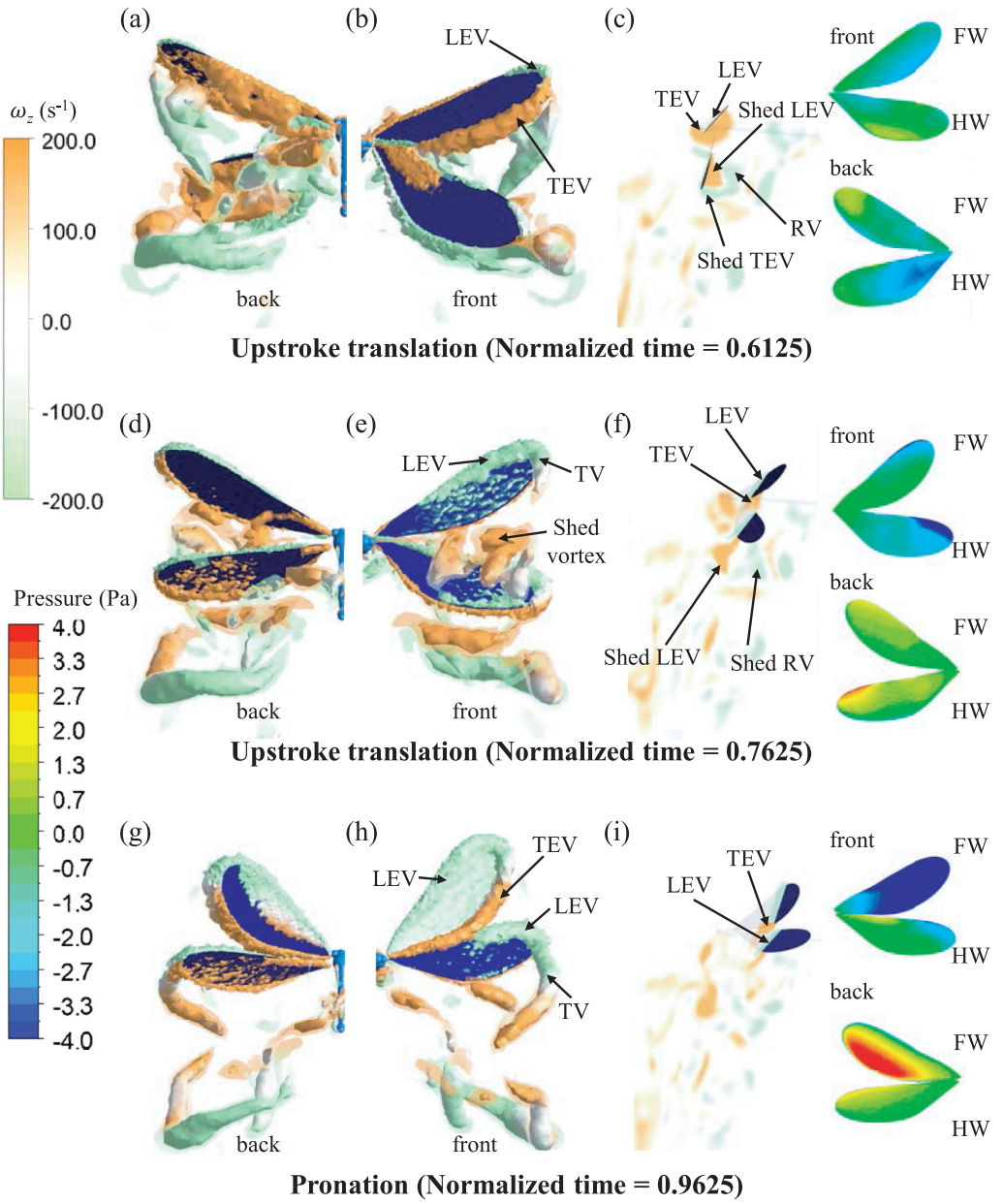

FIG. 13. Flow features of a damselfly hovering visualized with a Q criterion. (a,b) represent the flow features at normalized time 0.6125 from back and front views, respectively. (c) Flow feature at normalized time 0.6125 from a side view. (d,e) represent the flow features at normalized time 0.7625 from back and front views, respectively. (f) Flow feature at normalized time 0.7625 from a side view. At normalized time 0.9625 (g,h) show the flow features from back and front views, respectively. (i) Flow feature at normalized time 0.9625 from a side view.

to realize the vortex structure and to aid our analysis of the effect of the aerodynamic mechanisms. Three-dimensional flow fields were characterized with a Q criterion [37] defined as follows.

$$Q = \tfrac{1}{2}[|\boldsymbol{\Omega}|^2 - |\boldsymbol{S}|^2] \; > \; 0, \tag{11}$$

in which $S = \frac{1}{2}[\nabla \boldsymbol{u} + (\nabla \boldsymbol{u})^{\mathrm{T}}]$ is the strain rate tensor and $\Omega = \frac{1}{2}[\nabla \boldsymbol{u} - (\nabla \boldsymbol{u})^{\mathrm{T}}]$ is the vorticity tensor. In our work, the vortex structures of the damselfly and dragonfly were identified on plotting the 3D isosurface values of the Q criterion with Q = $3.5 \times 10^4 \mathrm{s}^{-2}$ and Q = $7.4 \times 10^4\ \mathrm{s}^{-2}$, respectively.

In the upstroke of a damselfly, the vertical force is produced steadily. As shown in Figs. 13(a) and 13(b), at normalized time 0.6125, the leading-edge vortex (LEV) and the trailing-edge vortex (TEV) begin to grow at the wing tip after the residual vortex leaves the upper surface during supination. As the upper surface can maintain a stable area of low pressure, the vertical force production of the fore wing begins to stabilize. The old tip vortex (TV) and old LEV separate from the wing tip at the bottom surface. There is no vortex attached at the wing tip, which causes a region of high pressure. The generation of a vertical force is obstructed also by the production of a root vortex (RV) of the hind wing in supination and many vortices attached to the bottom surface. From the

side view in Fig. 13(c), the LEV and the TEV on the upper surface of the fore wing begin to form and the vortex on the bottom surface begins to detach; the vertical force is stably increased. In contrast, the RV and the shed LEV of the bottom surface of the hind wing decrease the pressure difference between the upper and bottom surfaces.

At normalized time 0.7625 [Figs. 13(d) and 13(e)], the shed RV and the shed LEV are broken and separated. The vertical force increases obviously because the hind wing LEV is rapidly developed. From the side view in Fig. 13(f), the LEV and the TEV at the upper surface of the fore and hind wings can be clearly seen; they cause a significant pressure difference and thus increase the vertical force. At normalized time 0.9625 [Figs. 13(g) and 11(h)], the fore wing is in pronation and the hind wing is in upstroke. The fore wing TEV and the hind wing LEV affect each other, which causes the hind wing LEV to weaken; the pressure difference between the upper and bottom surfaces is thereby decreased. While the fore wing vortex thus does not appear at the trailing edge, it attaches completely to the upper surface. As a result, the pressure difference is enhanced; a maximum of vertical force occurs because of the effect of the wing rotation. From the side view in Fig. 13(i), because the fore wing and the hind wing are near, the fore wing TEV and the hind wing

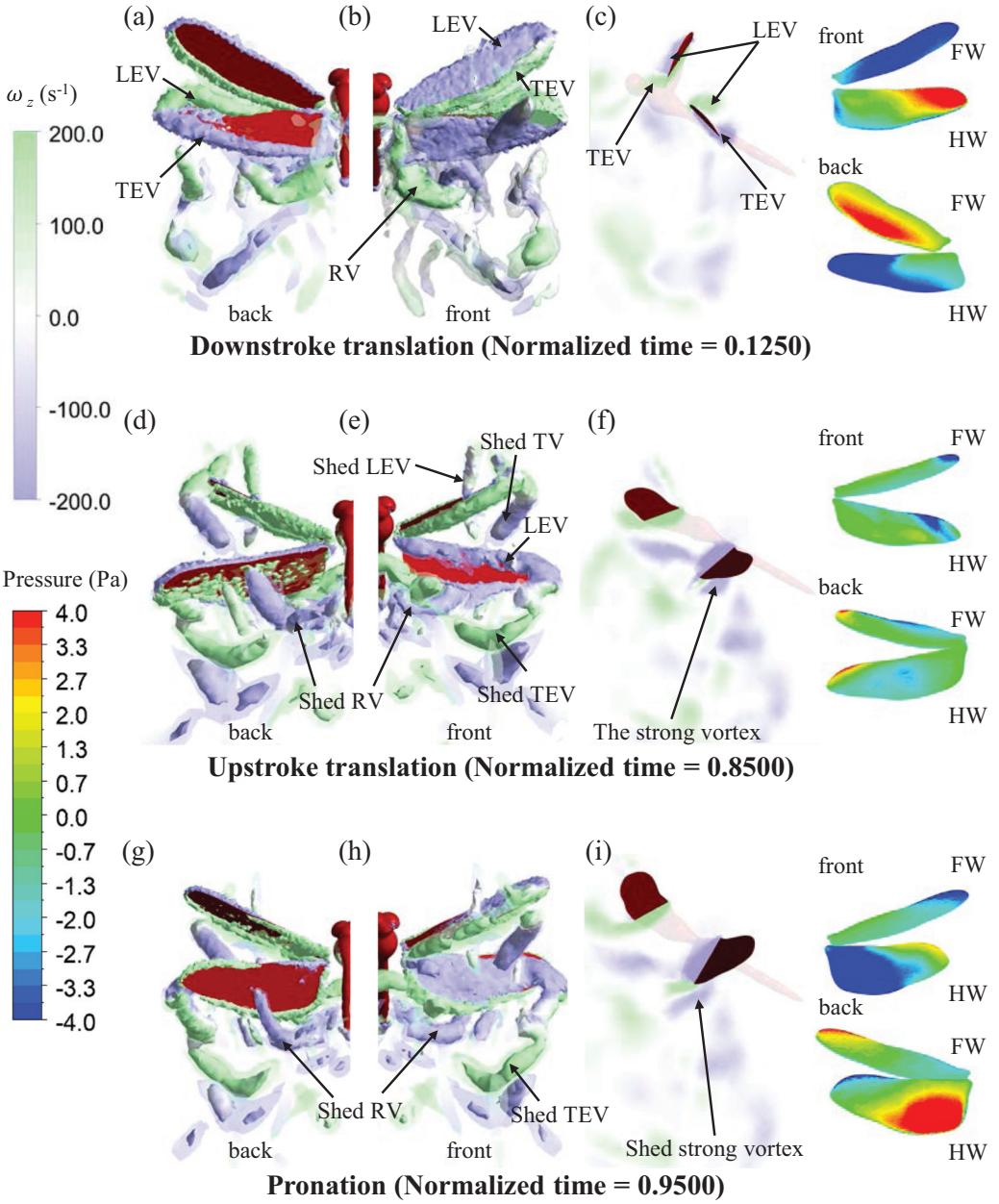

FIG. 14. Flow features of a dragonfly hovering visualized according to a Q criterion. (a,b) represent flow features at normalized time 0.1250 from back and front views, respectively. (c) Flow feature at normalized time 0.1250 from a side view. (d,e) represent flow features at normalized time 0.8500 from back and front views, respectively. (f) Flow feature at normalized time 0.8500 from a side view. At normalized time 0.9500, (g,h) show the flow features from the back and front views, respectively. (i) Flow feature at normalized time 0.9500 from a side view.

LEV produce a destructive interaction and thereby weaken the vortex on the upper surface of the hind wing, which causes a decreased pressure difference of the hind wing. The mechanism of the wing-wing interaction also was employed in other studies [17,31,32].

Further, Fig. 14 shows the flow field of a dragonfly hovering with normalized time (t/T). At normalized time 0.1250 [Figs. 14(a) and 14(b)], the dragonfly has a maximum vertical force, which benefits from the leading-edge vortex (LEV) on the pronation of the hind wing and the fore wing. From the side view in Fig. 14(c), the hind wing LEV and TEV begin to develop on the upper surface during a transition between pronation to downstroke translation whereas the fore wing LEV and TEV are enhanced during pronation. The fore and hind wings can hence produce a stable vertical force.

At normalized time 0.8500 [Figs. 14(d) and 14(e)], the shed LEV of the fore wing obstructs the new LEV generation, which causes a region of low pressure on the bottom surface; in this condition, the fore wing can produce no vertical force. The hind wing is disturbed by the strong vortex structure, which comprises the shed LEV, the wing-tip vortex (TV), the TEV of the fore wing, and the root vortex (RV) of the hind wing. The wing-root vortex generates during a wing rotation and sheds at the end of a wing rotation. A strong vortex structure is attached to the bottom surface of the hind wing; only a smaller LEV is attached to the upper surface. A vertical force can therefore not be generated effectively. From the side view in Fig. 14(f), a strong vortex can also be seen under the bottom surface of the hind wing, which decreases the pressure difference of the hind wing.

This strong vortex structure maintains its attachment until the hind wing pronation at normalized time 0.9500 [Figs. 14(g) and 14(h)]. When the strong vortex is shed, the hind wing LEV is rapidly developed. The generation of a vertical force increased because of the wing rotation. The shedding strong vortex can be seen also in Fig. 14(i). Movies of the flow field analysis are available in the Supplemental Material [38].

According to the flow structure, the wake generated by the fore wing of a dragonfly stays near the hind wing; the vertical force production of both wings thus decreases. In contrast, the vertical force produced by a damselfly is still stable in the upstroke because of the rapid detachment of the wake of the fore wing; its hind wing LEV could thus be developed. According to Phillips *et al.* [21], the LEV might detach readily on more petiolation during the upstroke. This phenomenon is used also to explain the flow structure in our work.

In the flight of an insect, the vortex structure around the wings plays an important role in the generation of an aerodynamic force. As mentioned above, the flow field of a dragonfly shows that a wing root vortex is obviously produced behind the wings. The RV is generated at the beginning of the stroke and detached during the stage of wing rotation. The separated RV then connects with the shed vortex ring to form a strong vortex structure, which might interfere with the generation of the vertical force of the fore and hind wings. The rapid rotation of the wing of a dragonfly along the spanwise axis might assist the attached vortex to separate from the wing surface because of the centrifugal force; the rotational effect would also compensate for the loss of the vertical force. For presumably these reasons a dragonfly hovers with a longer wing rotation and a larger amplitude of wing rotation. Although a damselfly might be able to benefit from the rotational effect, the rotational amplitude is somewhat smaller than for a dragonfly. As the vertical force is stably generated in the translation of both downstroke and upstroke, a damselfly adopts a longer stage of wing translation with a larger amplitude of flapping.

TABLE IV. Four cases in simulation with the combinations of different morphologies and kinematics.

Case	Morphology	Motion	Frequency	Vertical force/ body weight
Case 1	Damselfly	Damselfly	Damselfly	1.14
Case 2	Dragonfly	Dragonfly	Dragonfly	1.04
Case 3	Damselfly	Dragonfly	Damselfly	0.69
Case 4	Dragonfly	Damselfly	Dragonfly	1.87

To validate the correlation between the kinematics and the morphology, we implemented and compared the force and flow fields on the dragonfly morphology with the damselfly kinematics, and the damselfly morphology with the dragonfly kinematics. These analyses of force and flow fields are available in the Supplemental Material [38]. Notably, we alternated only the motions of the damselfly and the dragonfly, while maintaining their flapping frequencies to ensure that such results are caused by differences in motions. The ratios of the vertical force to the body weight are displayed in Table IV. We found that, no matter which morphology we used, the vertical force is better as long as it matches the damselfly kinematics. This result indicates that the motion of the damselfly is more beneficial to enhance the vertical force; the reason is that the motion of the damselfly has a large translational stage, which makes the vortex develop stably. The damselfly morphology with the dragonfly kinematics cannot produce a sufficient vertical force to support the body weight; the dragonfly morphology with the damselfly kinematics could have a larger vertical force to fly upwards. These artificial combinations are unsuitable for hovering. These results could explain why the damselfly and dragonfly use unique flight motions in their hovering strategies.

IV. CONCLUSION

The differences in biological morphologies of a damselfly and a dragonfly are innate conditions, beyond alteration, which might motivate these species to adopt distinct hovering strategies. Our purpose was hence to compare the differences in hovering kinematics and aerodynamics that could relate to differences in the wing morphologies between a dragonfly and a damselfly. We undertook experimental observations to investigate the wing kinematics of damselflies and dragonflies in hovering flight. Based on these experimental data, we applied an approximate function to quantify the flight motion, which enabled us to compare effectively the difference of flight kinematics. Numerical models of a damselfly and a dragonfly in hovering flight were created to analyze their flow structure and their generation of aerodynamic force. The experimental results revealed that a damselfly hovers with its fore wing in the lead, whereas a dragonfly hovers with its hind

wing in the lead. A damselfly flies with a smaller wing-beat frequency and a greater amplitude of flapping; its fore and hind wings beat with distinct stroke plane angles. In contrast, the flapping frequency of a dragonfly tends to be greater, with a greater variation of the rotation angle; the trajectories of the fore and hind wings are almost parallel during the flapping, as the angle of the wing stroke plane is similar [19]. As to wing morphologies, the wing of the damselfly is petiolate, which represents that the wing root is narrower than that of the dragonfly.

The results of the simulation showed that the force generation in the fore wing of both a damselfly and a dragonfly benefit from the LEV and TEV. The maxima of the vertical force caused by the rotational effect are significant. The wing-wing interaction is also an important mechanism. The same direction of the rotation of the vortex can produce constructive benefits, which might enhance the strength of the vortex. In contrast, the destructive offset with two vortices rotating in opposite directions weakens the vortex strength when the fore and hind wings are near each other [17,31,32]. Their root vortices appear at the trailing edge of the wing root during the wing rotation in the two cases, which might connect with other shed vortices to interfere with the LEV attachment.

Our results revealed that the flight pattern with a fore wing in lead or a hind wing in lead, respectively, could produce sufficient lift to balance the body mass, but the variation of wing morphologies might affect the root vortex attached. The root vortex of the damselfly detaches rapidly and has little effect on the generation of the flow structure; the vortex structure hence results in the generation of a steady vertical force during the upstroke. A damselfly hovers with a greater flapping amplitude and a longer phase of wing translation to obtain a steady generation of vertical force. In contrast, after the root vortex of a dragonfly is shed from the hind wing, it connects with the shed vortices of the fore wing to form a strong vortex structure. These vortices are trapped near the hind wing, which impedes the generation of a vertical force during the upstroke. A dragonfly thus hovers with a large rotational amplitude to assist the root vortex to separate from the wing surface. The rotational effect can supplement the lack of vertical force during the translational phase. The large flapping frequency can also replenish quickly the loss of a vertical force. In addition, through our verification of the alternating wing kinematics, we found that the damselfy kinematics is beneficial for enhancing the vertical force, because the motion of the damselfly has a large translational stage that allows the vortex to develop steadily. Alternating wing kinematics is unsuitable for the original wing morphology. In this report, we explain how the distinct hovering kinematics effectively provides lift with a distinct wing morphology. The development of suitable wing kinematics based on the limitations of body structure has its own evolutionary rationale. Moreover, considering the generation of a sufficient vertical force in the design of a micro-aerial vehicle, the motion of damselfly could be an effective design template.

ACKNOWLEDGMENTS

National Taiwan University partially supported this work under a project with Contract No. NTU-CC-108L894201. We thank Dr. J. F. Ogilvie for suggestions and discussion.

[1] Y. H. Chang, S. C. Ting, C. C. Liu, J. T. Yang, and C. Y. Soong, Exp. Fluids **51**, 1231 (2011).
[2] J. Y. Su, S. C. Ting, Y. H. Chang, and J. T. Yang, J. R. Soc., Interface **9**, 1674 (2012).
[3] Y. H. Chang, S. C. Ting, J. Y. Su, C. Y. Soong, and J. Y. Yang, Phys. Rev. E **87**, 022707 (2013).
[4] J. Y. Su, S. C. Ting, Y. H. Chang, and J. T. Yang, Phys. Rev. E **84**, 012901 (2011).
[5] R. Å. Norberg, *Swimming and Flying in Nature* (Springer, Berlin, 1975), p. 763.
[6] D. E. Alexander, J. Exp. Biol. **109**, 379 (1984).
[7] M. Sun and S. L. Lan, J. Exp. Biol. **207**, 1887 (2004).
[8] G. Lai and G. Shen, Sci. China, Phys., Mech. Astron. **55**, 2167 (2012).
[9] H. Wang, L. Zeng, H. Liu, and C. Yin, J. Exp. Biol. **206**, 745 (2003).
[10] A. Azuma and T. Watanabe, J. Exp. Biol. **137**, 221 (1988).
[11] J. K. Wang and M. Sun, J. Exp. Biol. **208**, 3785 (2005).
[12] M. Sun and H. Huang, AIAA J. **45**, 508 (2007).
[13] Z. Hu and X. Y. Deng, Acta Mech. Sinica **30**, 787 (2014).
[14] X. Sun, X. Gong, and D. Huang, Arch. Appl. Mech. **87**, 521 (2017).
[15] Z. J. Wang and D. Russell, Phy. Rev. Lett. **99**, 148101 (2007).
[16] J. R. Usherwood and F. O. Lehmann, J. R. Soc., Interface **5**, 1303 (2008).
[17] K. B. Lua, H. Lu, X. H. Zhang, T. T. Lim, and K. S. Yeo, Phys. Fluids **28**, 121901 (2016).
[18] C. Hefler, H. H. Qiu, and W. Shyy, J. Exp. Biol. **221**, (2018).
[19] J. Wakeling and C. Ellington, J. Exp. Biol. **200**, 557 (1997).
[20] A. T. Bode-Oke, S. Zeyghami, and H. Dong, Bioinspiration Biomimetics **12**, 056006 (2017).
[21] N. Phillips, K. Knowles, and R. J. Bomphrey, Interface Focus **7**, 20160084 (2016).
[22] A. Shahzad, F.-B. Tian, J. Young, and J. C. S. Lai, Phys. Fluids **28**, 111901 (2016).
[23] H. Park and H. Choi, Bioinspiration Biomimetics **7**, 016008 (2012).
[24] Y. Zheng, Y. Wu, and H. Tang, Bioinspiration Biomimetics **10**, 016021 (2015).
[25] D. Rival, D. Schönweitz, and C. Tropea, Bioinspiration Biomimetics **6**, 016008 (2011).
[26] Y. H. J. Fei and J. T. Yang, Phys. Rev. E **92**, 033004 (2015).
[27] Y. H. J. Fei and J. T. Yang, Phys. Rev. E **93**, 033124 (2016).
[28] Y. J. Lee, K. B. Lua, and T. T. Lim, Bioinspiration Biomimetics **11**, 056013 (2016).
[29] M. H. Dickinson, F.O. Lehmann, and S. P. Sane, Science **284**, 1954 (1999).
[30] S. P. Sane and M. H. Dickinson, J. Exp. Biol. **205**, 1087 (2002).
[31] T. M. Broering and Y.-S. Lian, Acta Mech. Sin. **28**, 1557 (2012).

[32] A. R. Shanmugam and C. H. Sohn, J. Mech. Sci. Technol. **33**, 2725 (2019).
[33] A. R. Ennos, J. Exp. Biol. **142**, 49 (1989).
[34] X. L. Mou, Y. P. Liu, and M. Sun, J. Exp. Biol. **214**, 2832 (2011).
[35] G. Luo, G. Du, and M. Sun, AIAA J. **56**, 25 (2018).
[36] C. Li and H. Dong, Bioinspiration Biomimetics **12**, 026001 (2017).
[37] J. C. Hunt, A. A. Wray, and P. Moin, in *Proceedings of the 1988 Summer Program, Center for Turbulence Research, CA, United States* (NASA, United Sates, 1988), pp. 193–208, Retrieved from https://ntrs.nasa.gov/search.jsp?R=19890015184.
[38] See Supplemental Material at http://link.aps.org/supplemental/10.1103/PhysRevE.100.063102, which includes two figures and one movie.